Observation of subband resonances between high-energy states in a series of asymmetric double-quantum-well superlattice systems

M. Hosoda, M. Sato, Y. Hirose, T. Shioji, and J. Nohgi
Department of Applied Physics, Osaka City University, Sugimoto, Sumiyoshi-ku, Osaka 558-8585, Japan

C. Domoto
ATR Adaptive Communications Research Laboratories, Seika-cho, Soraku-gun, Kyoto 619-0288, Japan

N. Ohtani
Department Electronics, Doshisha University, Tatara-Miyakodani, Kyotanabe, Kyoto 610-0321, Japan
(Received 18 August 2005; published 28 April 2006)

We report subband resonances related to higher energy subbands in a series of GaAs/AlAs asymmetric double quantum well superlattice (ADQW-SL) systems under electric field. Various phenomena can be observed in these ADQW-SL systems, such as the Γ-X-Γ electron resonance and transport, hole subband resonance, phonon replica, and Γ-Γ anticrossings. These resonances greatly affect photoluminescence properties, photocurrent-voltage characteristics, and photocurrent impulse responses. We also investigated the X-Γ transfer mechanism in these systems.

DOI: 10.1103/PhysRevB.73.165329 PACS number(s): 73.21.Cd, 73.63.Hs, 78.67.De, 73.50.Bk

I. INTRODUCTION

So far subband resonances have mainly been investigated by using simple-structured semiconductor superlattices (SLs) that consist of identical quantum wells (QWs) and barriers through entire SL periods. An alternative approach is the use of asymmetric double quantum well superlattices (ADQW-SLs). Experimental results and their interpretation in these systems are complex but interesting. There have been some reports on resonances in ADQW-SLs, especially those related to Γ ground states and holes.[1–3] However, there have been few reports on resonances between higher energy subband states and related carrier transport. Examples of higher energy subbands include the X state in the barrier and the first excited state of the Γ state in QW. In this case, since the transition from the X state is indirect, photoluminescence (PL) measurements and photocurrent spectra cannot be used to detect X states. Moreover, observations of PL emission from higher energy Γ subbands are difficult due to weak PL intensity caused by fast carrier relaxation from the states.

We recently pointed out that the X state shows a noticeable influence on carrier transport in ADQW-SLs.[4,5] In these systems, carrier occupation in higher energy subbands is sufficiently high and can be detected by PL measurements. Consequently, subband resonances related to higher energy subbands are easily detected. In this paper, we show that various subband resonances between higher energy subbands and related carrier transports can be observed and analyzed by using a series of ADQW-SLs.

II. EXPERIMENTAL AND SAMPLE STRUCTURES

We used three samples whose names and undoped ADQW-SL structures are shown in Table I. As shown in Fig. 1(a), all ADQWs were constructed from a NB/WQW/WB/NQW of AlAs/GaAs/AlAs/GaAs, where NB is a narrow-width barrier, WQW is wide QW, WB is wide barrier, and NQW is narrow QW. The samples were grown on (100)-oriented n^+-GaAs substrates by molecular beam epitaxy; the growth sequence was an n^+-GaAs, an n-$Al_{0.4}Ga_{0.6}As$ clad layer, undoped ADQW-SL with 50 nm $Al_{0.4}Ga_{0.6}As$ undoped cladding layers on both sides, a p-$Al_{0.4}Ga_{0.6}As$ clad layer, and a p^+-GaAs cap.

The sample was fabricated into p-i-n diode mesas of 400 μm squares. Especially for photocurrent impulse response measurements, some samples were fabricated into 50 μm square mesas to reduce the RC time constant to less than 100 ps. Alloyed Au electrodes were prepared to apply the electric field to the intrinsic region, and ohmic contact was confirmed by examining the forward biased current-voltage characteristics. Built-in voltage corresponding to the flatband condition was about 1.5 V of the forward bias voltage for all samples. In this paper, forward bias is denoted with a "−" sign, the reverse direction of the bias is written as "+" voltage, and thus the flatband condition is denoted by −1.5 V.

A 633 nm cw HeNe laser or an 82 MHz repetition rate, 400 nm wavelength, 100 fs pulse width second harmonics light pulse of a Ti:Sapphire laser was used as the excitation source. The excitation light was injected from the p-cap side. Time-resolved photocurrent was measured with a sampling

TABLE I. Structures of sample superlattices. Sequence of GaAs/AlAs/GaAs/AlAs ADQW width is denoted from the side nearest the p cap. ML is monolayer width of GaAs and AlAs.

Name	ADQW width (ML)	Superlattice period	Main feature
A	10/4/16/18	20	Standard
B	11/4/15/18	22	PL from NQW-Γ_1
C	10/2/18/18	24	Existing Γ state interference

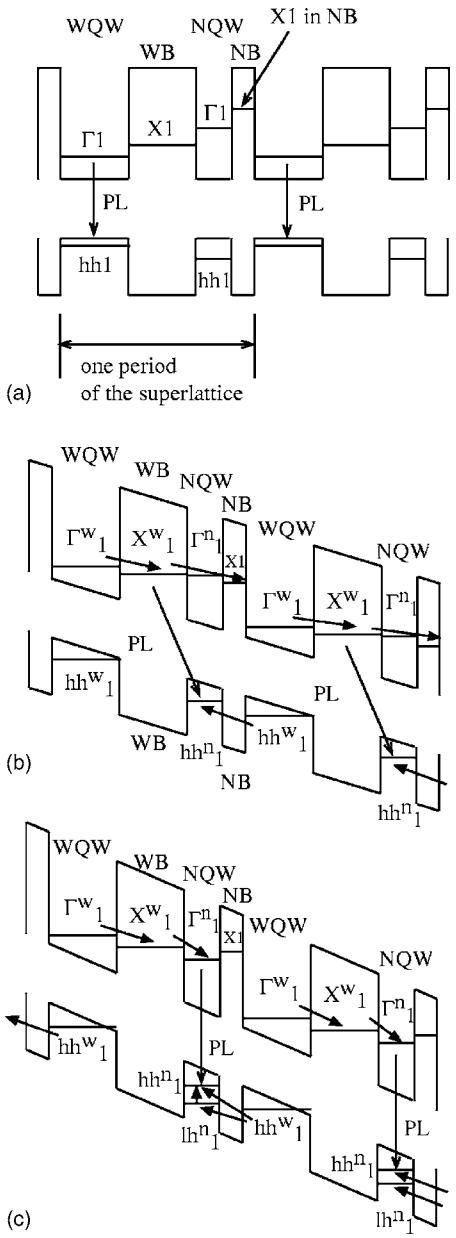

FIG. 1. (a) Schematic figures of subband energy structures of conduction and valence bands in ADQW-SLs under flatband conditions. Carrier transport under reverse bias voltage in samples *A* (b), and *B* (c), respectively (Ref. 6). Solid arrows indicate carrier transport and recombination transition. Only two periods in ADQW-SL are shown. The left direction is *p*-cap side of *p-i-n* diode.

oscilloscope. All data were measured at 20 K.

As shown in Fig. 1(a), the lowest conduction subband, i.e., Γ ground state (Γ_1) in NQW, is type-II aligned under flatband conditions. Therefore, photogenerated electrons and holes in the NQW relax into the WQWs through the NB. As shown in Figs. 1(b) and 1(c), when an electric field is applied, the electrons and holes in the WQW are transported inversely into the next NQW.

In the sections below, we use the following abbreviations to note the subband states. The first character shows the name of the subband state, the superscript denotes the position where the subband stays, and the subscript indicates the order of the subband state. The order number of the ground state is one. For example, Γ_1^w indicates ground Γ state in WQW, Γ_2^w indicates the first excited Γ state in WQW, X_1^n is ground *X* state in narrow barrier (NB), and hh_1^w is ground *hh* state in WQW.

III. PL PROPERTIES

Figure 2 shows the PL spectra of three samples as a function of reverse bias voltage. Since the PL spectra of samples *A* and *B* in Figs. 2(a) and 2(b) were previously described in Ref. 5, we omit descriptions and only explain their essence. X_1^w-hh_1^n PL is X_1 Stark-ladder PL [cf. Fig. 1(b) and Ref. 5]. This PL emission is caused by Γ-*X* mixing with the Γ_1^n state. Simultaneously, this ADQW system allows inverse hole transfer from WQW to NQW through NB. Therefore, radiative recombination to the hh_1^n state occurs under sufficiently high bias voltages.

Γ_1^n-hh_1^n is PL emission from NQW. This PL cannot be observed in sample *A* because Γ_1^n-X_1^n resonance occurs before X_1^w-Γ_1^n resonance with increasing bias voltage. When X_1^w-Γ_1^n resonance occurs, since X_1^n energy is already lower than Γ_1^n energy, electrons in the Γ_1^n state are rapidly retrapped into the X_1^n state and transferred to the next ADQW [cf. Fig. 1(b)]. Reduced electron occupation is not sufficient to emit Γ_1^n-PL. On the other hand, in samples *B* and *C*, Γ_1^n-X_1^n transfer occurs after X_1^w-Γ_1^n resonance [cf. Fig. 1(c)]. Therefore, sufficient Γ_1^n PL can be observed, caused by electron relaxation from X_1^w into Γ_1^n. Electron occupation in the Γ_1^n state is promoted after LO-phonon energy (36 meV) separation between the X_1^w and Γ_1^n states, and Γ_1^n PL emission is sustained until the Γ_1^n-X_1^n transfer opens [cf. Fig. 2(b)].

A. Verification of carrier transport from WQW to NQW

Figure 3 shows NQW PL in sample *B* under 730 nm cw Ti:Sapphire laser excitation. In contrast to 633 nm HeNe laser excitation, a 730 nm light only generates photocarriers in the WQW. Therefore, NQW PL is evidently generated by the transferred electrons and holes from WQW into NQW due to Γ_1^w-X_1^w-Γ_1^n electron transfer and hole tunneling from WQW to NQW. Moreover, the voltage range for observing NQW PL agrees well with that under HeNe laser excitation. This fact indicates that the carrier transport model is still available under HeNe laser excitation.

B. Interference between subband states in WQW and NQW

Figure 2(c) shows the PL spectra of sample *C*. The brightness shows logarithmic PL intensity (base=10). In the PL image, intensity shorter than 720 nm wavelength is 100 times magnified to clarify weak PL emission. Complex PL behavior originates from phonon replica, interwell transition, and state interference between higher energy subbands.

Figure 4 shows the energy fancharts of the electron and hole subbands in sample *C*. Note that interference related to the first excited Γ state in WQW (Γ_2^w), which will be described below, has not yet been included. Figure 4 shows two different views for energy shift. In ADQW systems, since the

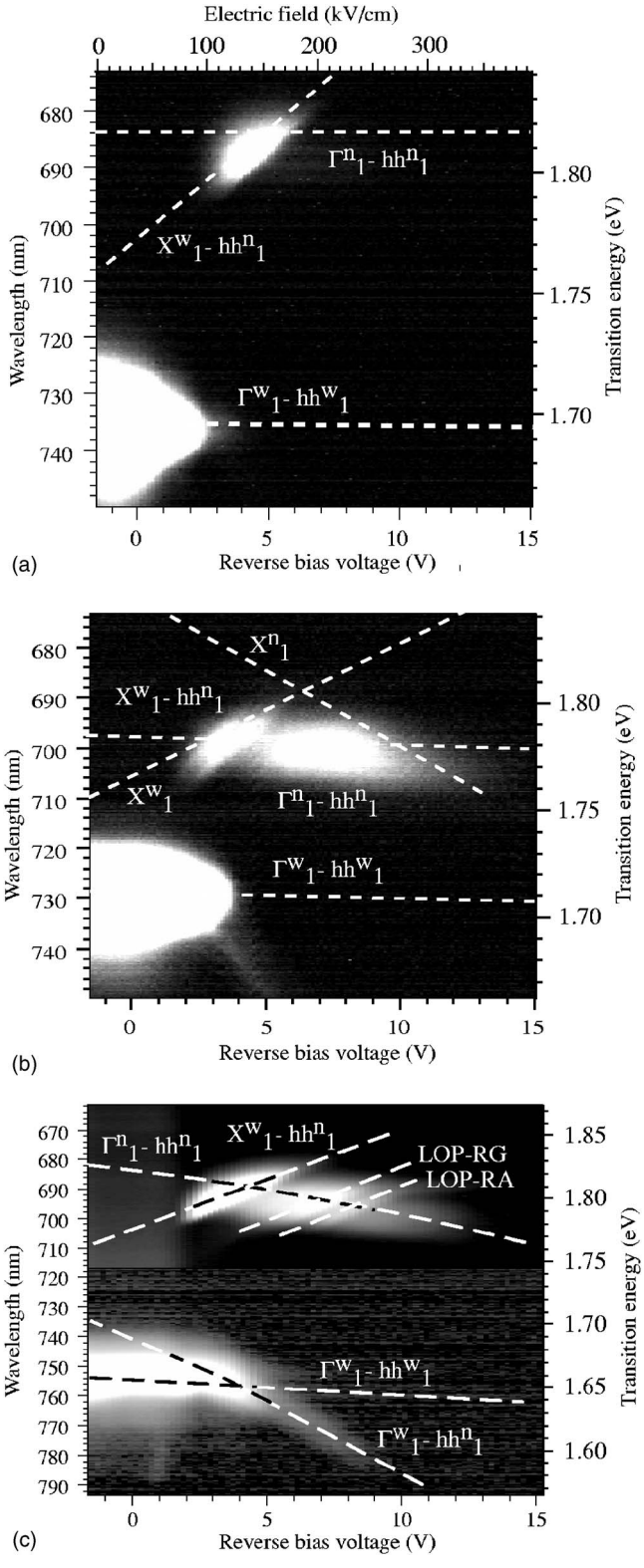

FIG. 2. PL spectra of samples *A* (a) (Ref. 6), *B* (b) (Ref. 6), and *C* (c) as a function of reverse bias voltage under 0.1 mW HeNe laser excitation. Brightness (gray level) represents PL intensity. Brightness of image is clipped at higher intensities to clearly show weak PL areas. Dotted lines show calculated energies including exciton binding energy of 5 to 10 meV.

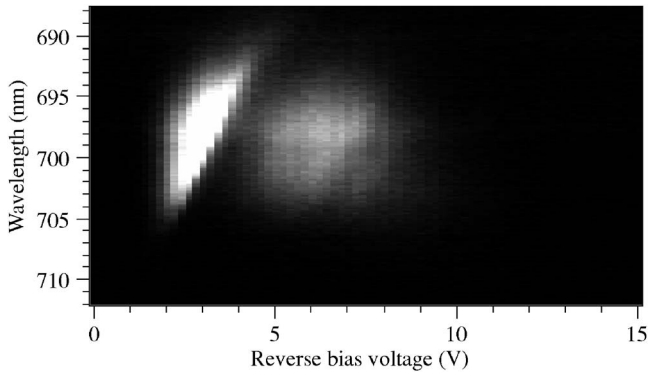

FIG. 3. PL spectra from higher energy subbands in sample *B* as a function of reverse bias voltage under 0.1 mW 730 nm Ti:Sapphire laser excitation.

value of energy shift depends on the selections of the center base QW, there are two viewpoints. One is energy shift versus WQW, and the other is versus NQW. Figures 4(a) and 4(b) denote the energy shift of the electron and hole subbands viewed from center base WQW. In these figures, the energies of the WQW subbands do not shift, while NQW subbands show energy shift as Stark-ladder states. Figures 4(c) and 4(d) are fancharts viewed from NQW. Here, WQW subbands show Stark shift. These four energy charts are necessary to analyze interwell transitions.

Anomalously redshifted Γ^w_1 PL around 770 nm and 7 V originates from Γ^w_1-hh^n_1 radiative recombination, which is a spatially indirect transition through the 2 ML thin barrier. From Fig. 4(d), the hh_1 states in WQW and NQW show large anticrossing around 3.5 V due to wave function interference through the 2 ML AlAs barrier. After this crossing, the hh^n_1 energy lowers hh^w_1, and then most of the holes in the WQW are transferred into NQW. Consequently, Γ^w_1-hh^n_1 spatially indirect interwell transition occurs. Since the energy shift of the hh^n_1 line in Fig. 4(b), which is viewed from the center base WQW, shows a linear shift, a Γ^w_1-hh^n_1 PL is observed as a Stark-ladder PL. The Γ^w_1-hh^n_1 PL is observed as a branch of the Γ^w_1-hh^w_1 PL, as shown in Fig. 2(c).

PL spectra observed around 5 V and 690 nm are X^w_1 Stark-ladder PLs. Since the holes have already been transferred into NQW from 3 V, this X^w_1 PL transition occurs between the X^w_1 and hh^n_1 states. Observed PL energy agrees well with the calculated energy of the X^w_1-hh^n_1 transition from Figs. 4(c) and 4(d).

PL lines indicated as LO-RG and LO-RA are phonon replica of the X^w_1-hh^n_1 transition. The energy separations of the LO-RG and LO-RA PL lines from the X^w_1-hh^n_1 PL agree well with the GaAs Γ(36 meV) and AlAs Γ(50 meV) LO-phonon energies, respectively. Since the X^n_1 energy in sample *C* is much higher than other samples, Γ^n_1-hh^n_1 PL continues during relatively long voltage ranges. Therefore, PL from the phonon replica can easily be observed.

Although most PL behaviors can be explained by the fancharts in Fig. 4, anomalous redshift of the Γ^n_1-hh^n_1 PL cannot be explained. The observed Γ^n_1-hh^n_1 PL from 5 V shows larger redshift than the energy shift derived from the fancharts. The Γ^n_1-hh^n_1 transition shows no Stark-ladder shift,

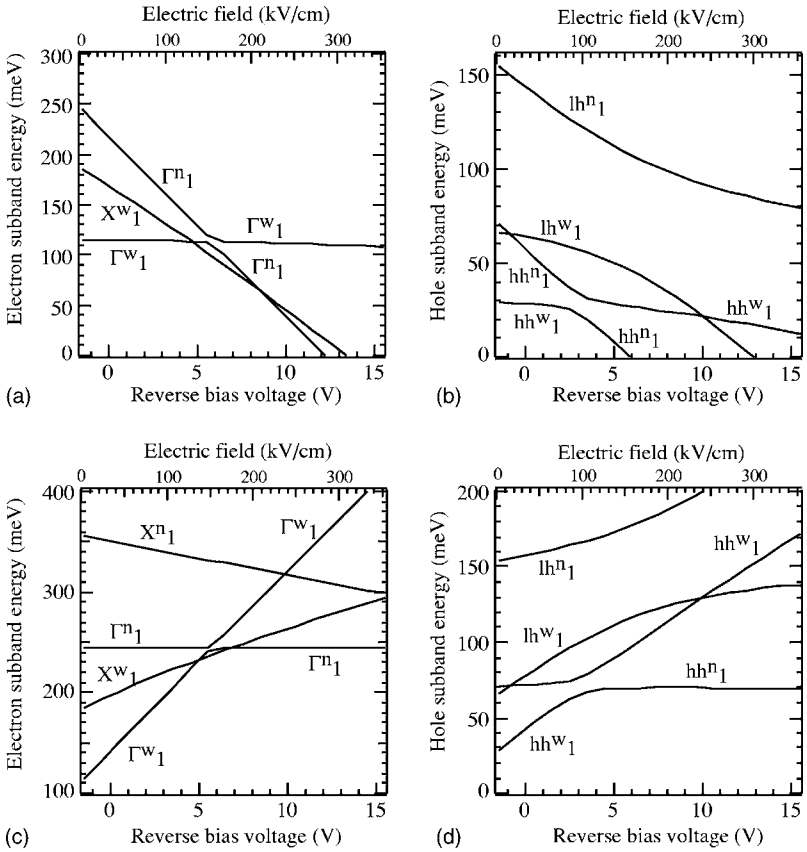

FIG. 4. Calculated subband energy fancharts of sample *C*. Figures (a) and (b) denote energy shift of electron and hole subbands viewed from center base WQW. Figures (c) and (d) are identical fancharts viewed from NQW. Although calculation excludes interference between *lh* and *hh*, such omission does not affect the analysis of this report.

since the transition occurs *in the same QW*, and thus the Γ_1^n-hh_1^n transition energy is calculated using the energy lines in Figs. 4(c) and 4(d). This additional redshift originates from the additional interference between the Γ_1^n and Γ_2^w states. Since sample *C* has a very thin barrier, i.e., 2 ML NB, for separating NQW and WQW, interference between the Γ wave function in WQW and in NQW cannot be ignored. In this case, anticrossing becomes very large, which greatly deviates the subband energy. Figure 5 shows the correction of the Γ_1^n energy under anticrossing between the Γ_2 state in WQW and Γ_1 state in NQW. The corrected fanchart explains the anomalous redshift in Γ_1^n PL. The dotted line for Γ_1^n-hh_1^n PL in Fig. 2(c) shows transition energy corrected by the Γ_1^n-Γ_2^w interference in Fig. 5 and agrees well with experimental results. This result shows that the interference of the wave function through the thin barrier in ADQW systems strongly affects the energy level of the ground subband state. Although such interferences and anticrossings have been detected by measurements such as photocurrent spectra, few reports have used PL measurements, since carrier occupation in higher energy subbands is usually very small. By using properly designed ADQW-SL systems, we can clearly detect this interference by PL measurements.

C. *X*-Γ transfer mechanism

It has been reported that Γ-*X* transfer is dominantly caused by electron scattering by interface roughness.[7] In contrast to Γ-*X* transfer, however, controversy exists whether *X*-Γ transfer is caused by interface roughness or phonon-assisted transport. In our previous reports on X_1-Γ_2 transfer, interface roughness was consistent with experimental results.[8–10] However, our experimental results in this report show that LO-phonon assisted transport dominates *X*-Γ transfer. We believe that this discrepancy in *X*-Γ transfer mechanisms arises from the following differences in reso-

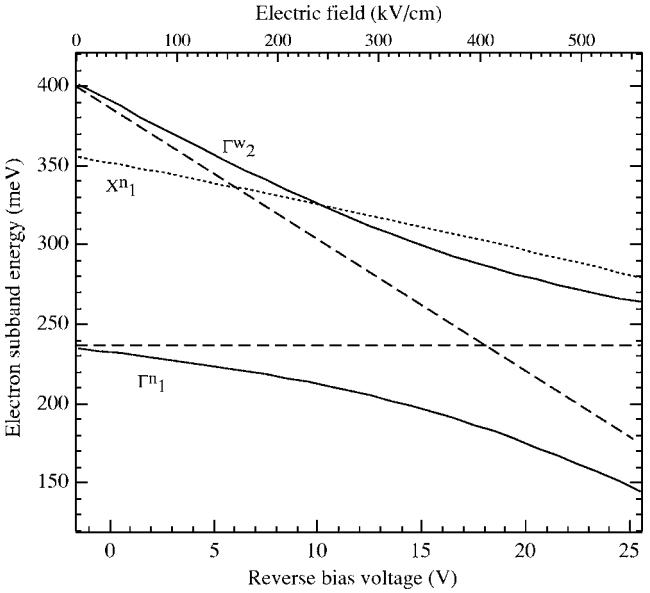

FIG. 5. Calculated subband energy fanchart of sample *C* including wave function interference between WQW and NQW Γ states separated by 2 ML thin barrier.

nance conditions. The previous reports addressed X_1-Γ_2 transfer. In this case, the destination of the transfer is the Γ_2 state, so transferred electrons can relax further. Relaxation from the Γ_2 to the Γ_1 state in the same QW can contain a multiple LO-phonon emission process. Therefore, discrepancy in the momentum between the X_1 and Γ_2 states might be adjusted by a transition among a three-level system, i.e., X_1-Γ_2-(LO-phonon emission). In contrast, the destination in this report is the ground Γ state, so electrons cannot relax to any other Γ states in the same QW. Therefore, the above three-level relaxation process cannot work. The only possible relaxation is spatially indirect transition. Therefore, it is concluded that when there is no spatially direct relaxation path from the destination, i.e., from the ground Γ state, X-Γ transfer is promoted by LO-phonon emission, not by interface roughness. Note that the Γ-X transfer mechanism in our sample is consistent with the previous interface roughness theory.

Our experimental results indicate an additional finding. Even though the barrier is very thin, the X state in NB sufficiently operates as a quantum state in the Γ-X transfer. This function operates up to a 2 ML width barrier in sample C. Therefore, the function of the Γ-X transfer is strong enough and must be considered in carrier transport even under very thin barrier widths.

There is an another finding. Γ_1^n PL in sample B is promoted after 36 meV LO-phonon energy separation between the X_1^w and Γ_1^n states at about 7 V, and its intensity decreases from 10 V due to the Γ_1^n-X_1^n transfer. However, Γ_1^n PL continues up to 13 V, where energy separation between the Γ_1^n and X_1^n states increases more than the 36 meV LO-phonon energy, and thus LO-phonon assisted Γ_1^n-X_1^n transfer starts. Therefore, the escape of electrons from the Γ_1^n state is further promoted, terminating Γ_1^n PL emission. From this result, LO-phonon assisted Γ_1-X_1 transport coexists with transport by interface roughness and still exists even under thin barrier conditions.

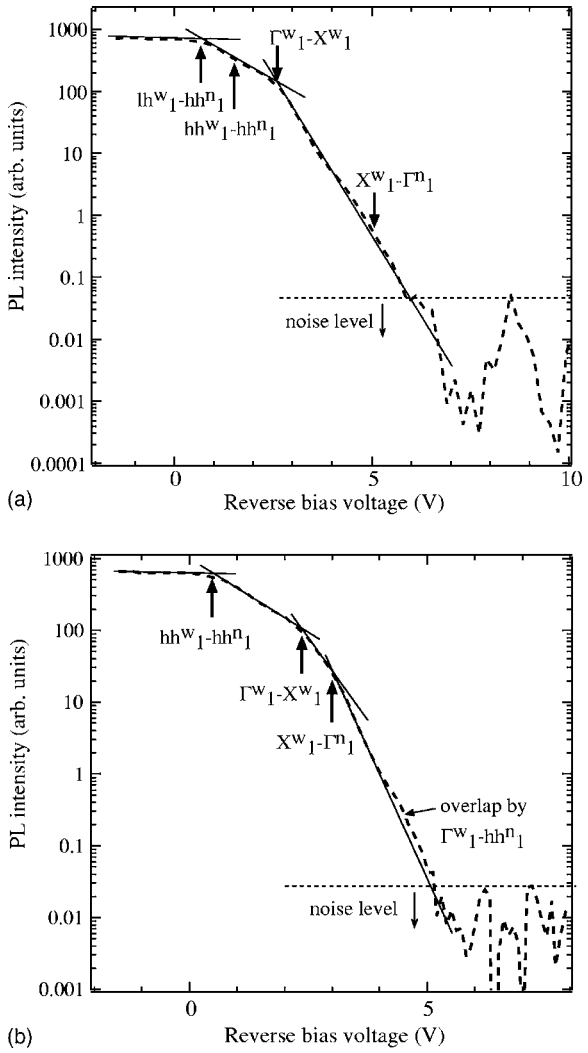

FIG. 6. WQW Γ_1 PL intensity as a function of reverse bias voltage of samples A (a) and B (b) under 1 mW HeNe laser excitation. Vertical intensity axis is logarithmic with base=10.

IV. RESONANCES THAT APPEARED IN THE PL INTENSITY OF WQW

Subband resonances can also be observed in a characteristics curve of PL intensity against the applied electric field. Figure 6 shows the logarithmic plots of Γ_1^w PL intensity of sample A and B as a function of reverse bias voltage. Since the PL intensity of sample C shows similar characteristics, we omit the explanation. Arrows indicate the related subband resonances. Γ_1^w PL intensity dominantly depends on both electron and hole occupations in the Γ_1 and hh_1 states in WQW. Occupation is reduced by the escape of the carriers, which is caused by resonances. Therefore, PL intensity reflects the resonance and the followed carrier transport, a phenomenon commonly known as the quenching of PL intensity due to carrier sweep-out from the SL active region.

In Fig. 6(a), there are two traces of resonance. The first kink, i.e., the change point of the derivative of the curve at about 0.5 V, is identified as the opening of the lh_1^w-hh_1^n transfer. The second point at about 2.5 V is identified as the start of the electron trap into X_1^w from Γ_1^w. Once an electron is captured from the Γ_1 state into a type-II aligned X_1 state in the barriers, the electron will stay there for a relatively long period of X_1-Γ_1 relaxation.[11] This trapping of electrons is released by the X_1^w-Γ_1^n resonance indicated by the weak shoulder at about 5 V. This resonance point is relatively clear in Fig. 6(b) as the third kink near 3 V. After this resonance, since the trapped electrons in X_1^w can escape to Γ_1^n, sweep-out speed from the active SL region increases due to the Γ_1^w-X_1^w-Γ_1^n-Γ_1^w transfer, further promoting PL quenching.

In contrast to sample A, sample B has a clear trace of X_1^w-Γ_1^n transport, as shown in Fig. 6(b). It comes from the difference in the function of X_1^n on electron transport, as described in Sec. III. The first kink at about 0.5 V corresponds to the opening of the hh_1^w-hh_1^n transfer. Since energy separation between the hh_1^w and lh_1^w states is much greater than sample A, holes cannot occupy lh_1^w at low carrier temperatures, and thus the lh_1^w-hh_1^n transfer observed in sample A does not happen. The shoulder at around 4.5 V originates from overlap by Γ_1^w-hh_1^n Stark-ladder PL, as described in Sec. III B. In fact, this PL can be seen in Fig. 2(b) from 3.5 V at

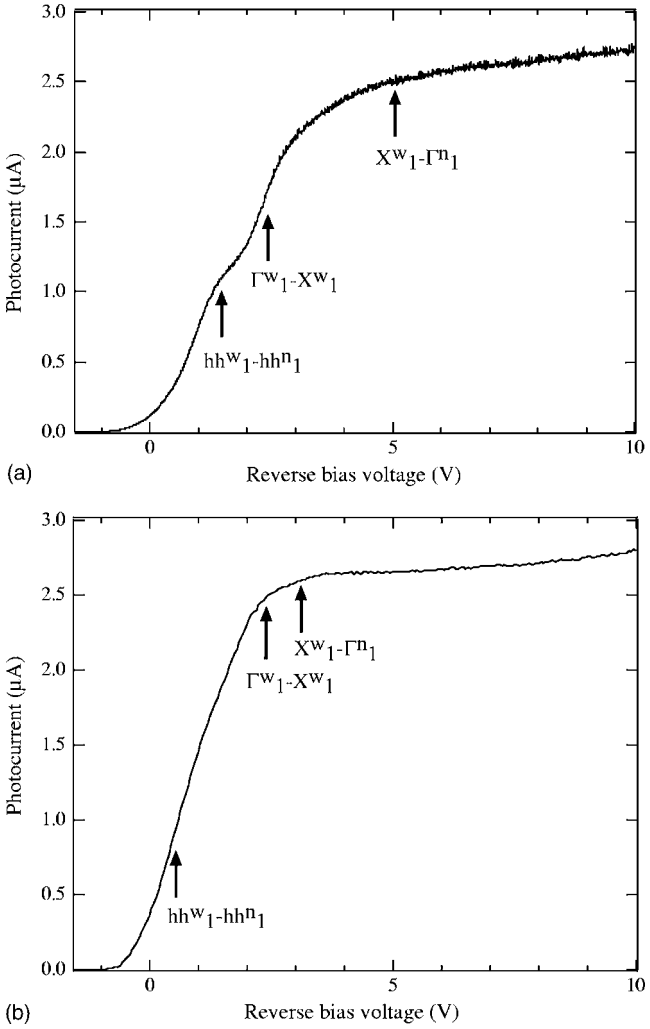

FIG. 7. Photocurrent versus reverse bias voltage characteristics (*I-V* curve) of samples *A* (a) and *B* (b) under 0.1 mW HeNe laser excitation.

around 745 nm as a very weak and anomalous tail of Γ_1^w-hh_1^w PL. This Stark-ladder PL is also observed more clearly in sample *C* [cf. Fig. 2(c)], since the Γ_1^w-hh_1^n interwell transition is more effective under less NB width.

V. RESONANCES THAT APPEARED IN PHOTOCURRENT-VOLTAGE CHARACTERISTICS

Evidence of subband resonances and related carrier transport is also observed in the photocurrent-voltage characteristics (*I-V* curve). However, the interpretation of the *I-V* curve is different from the PL curve. In contrast to Γ_1^w PL intensity characteristics that only monitor carrier occupation in WQW, the *I-V* curve represents the total average flow of photocarriers through the entire SL. Therefore, resonance points are relatively smeared, complicating their interpretation more than those in the Γ_1^w PL intensity curve.

From the *I-V* curve of sample *A* in Fig. 7(a), the first marker is identified as the hh_1^w-hh_1^n hole transfer and the second as the X_1^w-Γ_1^n electron transfer. Since both transfer processes promote carrier transport, photocurrent is increased toward these resonance voltages. However, in contrast to the Γ_1^w PL intensity characteristics, the resonance points are relatively smeared.

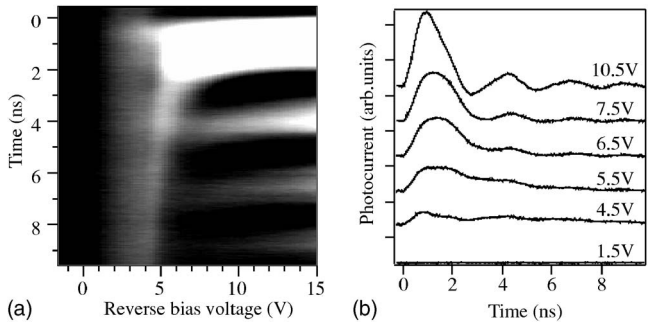

FIG. 8. (a) Time-resolved photocurrent response image (TIV graph) of sample *C*. Brightness represents photocurrent intensity. Gray level representing high current intensities is saturated to show lower level current intensity regions. (b) Time-resolved photocurrent response at various reverse bias voltages. Baseline of curve is intentionally shifted for clarity. Excitation source is 1 mW 400 nm 100 fs Ti:Sapphire laser.

In the *I-V* curve of sample *B* in Fig. 7(b), there are three related points. The shoulder at the first marker is identified as the hh_1^w-hh_1^n hole transfer and the second as the Γ_1^w-X_1^w electron transport. Since both transfer processes promote carrier transport, the photocurrent is increased toward these resonance voltages. The last marker indicates the X_1^w-Γ_1^n resonance. From here, photocurrent gradually increases since electron relaxation from the X_1^w state to the Γ_1^n state has started. As shown in Figs. 1(c) and 2(b), Γ_1^n PL is promoted at the 36 meV LO-phonon energy separation between the X_1^w and Γ_1^n states at 7 V, and its intensity greatly decreases from 10 V due to the Γ_1^n-X_1^n transfer. However, there is no clear trace of the above transport in the *I-V* curve because the carrier transport was already effective after the X_1^w-Γ_1^n transfer due to tunneling through the thin NB, even if the electrons do not relax into the Γ_1^n state. Since the *I-V* curve represents the total efficiency of carrier transport in the entire SL, the *I-V* curve cannot discriminate carrier path when two different paths have nearly equal efficiency.

For sample *C*, since a similar tendency to sample *B* was observed, we omit the figure.

VI. ANOMALOUSLY DELAYED COMPONENTS IN PHOTOCURRENT IMPULSE RESPONSE

In some SLs, anomalously delayed components, observed in photocurrent impulse responses,[8,10,12] originate from the escape process of the trapped electrons in *X* states. In the ADQW-SL systems in this report, the same phenomenon may arise since similar Γ-*X*-Γ transfer exists. In fact, we found anomalously delayed photocurrents in all samples.

Figure 8(a) shows the bias voltage dependence of time-resolved photocurrent response [Pc(*t*)] in sample *C*, that is, the time-resolved *I-V* characteristics (TIV graph) composed from Pc(*t*) at each bias voltage, as exemplified in Fig. 8(b). The brightness in the TIV graph represents photocurrent in-

tensity. "Time=0" denotes the starting time of the optical pulse excitation. Weak horizontal lines at 4.5 and 7 ns are spurious ringing signals caused by impedance mismatch of electric circuits. Since the penetration depth of the 400 nm excitation wavelength is very shallow, only an electron charge sheet runs through the intrinsic SL region, and thus only electron transport characteristics are observed.

In Fig. 8, a delayed component is observed in the voltage range from 4.5 to 7 V. From 4.5 V, the delayed component reduces delay with increasing bias voltage, and it finally converges to a single Pc(t) peak at 7 V. This behavior indicates the increasing escape rate of the trapped electrons in the X states to other quantum states. As shown in Fig. 4, electrons are captured from the Γ_1^w state into the type-II aligned X_1^w state from about 4.5 V and stay there for a relatively long period of X_1-Γ_1 relaxation.[11] In this case, Pc(t) will have a weak and slow tail, as exemplified by Pc(t) at 5.5 V in Fig. 8(b). The decrease in delay is caused by the opening of a new escape channel from the X_1^w state: the X_1^w-Γ_1^n path. As described in Sec. III C, X_1^w-Γ_1^n transfer is promoted when the energy separation between the X_1^w and Γ_1^n states exceeds LO-phonon energy (36 meV). This LO-phonon assisted transport is established from about 7 V. From this voltage, electrons can run through the SL with sufficient velocity, and thus the delayed components in the photocurrent vanish. The behavior of the delayed components derived from the above theory is consistent with the experimental results shown in Fig. 8.

VII. CONCLUSION

In summary, various types of resonances and related carrier transports among the ground and higher energy subband states were observed in a series of asymmetric double quantum well superlattices under electric fields. Γ-X-Γ electron transport and hole-hole tunneling transport were clearly identified in the experimental results for the reverse bias voltage characteristics of photoluminescence spectra, photoluminescence intensity, photocurrent, and photocurrent impulse response. Regarding electron transport from ground X state in the barrier to ground Γ state in the quantum well, we found that LO-phonon assisted transport dominates the X-Γ transfer. The Γ-X transfer function works enough even under very thin barrier widths. In addition, we experimentally observed that anticrossing caused by the interference between the ground and higher energy Γ subband states strongly affects the Γ ground state energy in the asymmetric double quantum well having a very thin barrier width.

ACKNOWLEDGMENT

Part of this study was supported by a Grant-in-Aid (No. 14350013) from the Ministry of Education, Culture, Sports, Science, and Technology of Japan.

[1] F. Agulló-Rueda, H. T. Grahn, and K. Ploog, J. Appl. Phys. **79**, 8106 (1996).
[2] L. Schrottke, R. Hey, and H. T. Grahn, Phys. Rev. B **60**, 16635 (1999).
[3] M. Takeuchi, K. Kawashima, and K. Fujiwara, J. Appl. Phys. **79**, 8106 (1996).
[4] C. Domoto, N. Ohtani, K. Kuroyanagi, P. O. Vaccaro, H. Takeuchi, M. Nakayama, and T. Nishimura, Appl. Phys. Lett. **77**, 848 (2000).
[5] Y. Hirose, M. Hosoda, C. Domoto, T. Nishimura, and T. Aida, Appl. Phys. Lett. **81**, 3870 (2002).
[6] Y. Hirose, M. Hosoda, C. Domoto, T. Nishimura, and T. Aida, reprinted with permission from Appl. Phys. Lett. **81** (20), 3870 (2002), Copyright 2002, American Insitute of Physics.
[7] *Optics of Semiconductor Nanostructures*, edited by F. Henneberger, S. Schmitt-Rink, and E. O. Göbel (Akademie Verlag, Berlin, 1993), Chapter 1–7; and references therein.
[8] M. Hosoda, N. Ohtani, H. Mimura, K. Tominaga, P. Davis, T. Watanabe, G. Tanaka, and K. Fujiwara, Phys. Rev. Lett. **75**, 4500 (1995).
[9] M. Hosoda, H. Mimura, N. Ohtani, K. Tominaga, K. Fujita, T. Watanabe, H. Inomata, and M. Nakayama, Phys. Rev. B **55**, 13689 (1997).
[10] M. Hosoda, N. Ohtani, H. Mimura, K. Tominaga, T. Watanabe, H. Inomata, and K. Fujiwara, Phys. Rev. B **58**, 7166 (1998).
[11] J. Feldmann, M. Preis, E. O. Göbel, P. Dawson, C. T. Foxon, and I. Galbraith, Solid State Commun. **83**, 245 (1992).
[12] M. Hosoda, K. Tominaga, N. Ohtani, H. Mimura, and M. Nakayama, Appl. Phys. Lett. **70**, 1581 (1997).